Time-dependent density-functional theory for molecular processes in strong fields: Study of multiphoton processes and dynamical response of individual valence electrons of N_2 in intense laser fields

Xi Chu and Shih-I Chu
Department of Chemistry, University of Kansas, and Kansas Center for Advanced Scientific Computing, Lawrence, Kansas 66045
(Received 30 July 2001; published 14 November 2001)

We present a time-dependent density-functional theory (TDDFT) with proper asymptotic *long-range* potential for nonperturbative treatment of multiphoton processes of many-electron molecular systems in intense laser fields. A *time-dependent generalized pseudospectral* method is extended for precision solution of the TDDFT equations for two-center diatomic systems. The procedure allows *nonuniform* optimal spatial grid discretization of the Hamiltonian in prolate spheroidal coordinates and a split-operator scheme in *energy* representation is used for the time propagation of the individual molecular spin orbital in space and time. The theory is applied to the first detailed *all-electron* study of multiphoton ionization and high-order harmonic generation (HHG) processes of N_2 in intense laser fields. The results reveal unexpected and intriguing nonlinear optical response behaviors of the individual valence spin orbital to strong fields. In particular, it is found that the dominant contribution to the total HHG power spectrum of N_2 is due to the constructive and destructive interferences of the induced dipoles of the two highest-occupied bonding $(3\sigma_g)$ and antibonding $(2\sigma_u)$ molecular orbitals in the presence of intense laser fields.

DOI: 10.1103/PhysRevA.64.063404 PACS number(s): 42.50.Hz, 71.15.Mb, 42.65.Ky, 33.80.Wz

I. INTRODUCTION

The study of atomic and molecular multiphoton processes in intense and superintense laser fields is a subject of much current interest in science and technology. To describe such strong-field processes using *ab initio* wave-function approach, it is necessary to solve the time-dependent Schrödinger equation of many-electron systems in space and time, which is beyond the capability of current computer technology. To overcome this bottleneck, time-dependent density-functional theory (TDDFT) with *self-interaction correction* (SIC) has been recently developed for nonperturbative treatment of many-electron atomic systems (particularly rare-gas atoms) in strong fields [1–3]. More recently, a self-interaction-free TDDFT formulation for molecular systems has also been developed and applied to the study of *multiphoton ionization* (MPI) and *high-order harmonic generation* (HHG) of H_2 molecule in intense laser fields [4]. In this paper, we extend the TDDFT to the study of multi-electron molecular systems (N_2 in particular) with an aim to explore the dynamical role and nonlinear response of *individual* electron spin orbital to the intense fields, a subject of largely unexplored area of strong-field molecular physics. Such a study can provide insights regarding detailed quantum dynamics and MPI/HHG mechanisms from each individual valence electron, as well as the optimal control of the strong-field processes of many-electron systems.

A central theme of modern TDDFT is a set of time-dependent Kohn-Sham like equations that are structurally similar to the time-dependent Hartree-Fock equations but include, in principle exactly all many-body effects, through a *local* time-dependent exchange-correlation (xc) potential [1–6]. In reality, the exact (steady-state or time-dependent) xc energy functional form is unknown. Thus, in actual DFT or TDDFT calculations, approximate xc energy functionals need to be used. It is well known, however, that the explicit xc energy functionals commonly used, such as those of *local spin-density approximation* (LSDA) or the more refined *generalized gradient approximation* (GGA), contain spurious self-interaction energy [7]. As a consequence, the resulting one-particle xc potentials do not possess the proper long-range Coulombic $(-1/r)$ behavior. For example, the one-particle LSDA potential decays exponentially and the electrons are too weakly bound, and for negative ions even unbound. Thus, while the total energies of the ground states of atoms predicted by these explicit (LSDA/GGA) xc energy functionals are rather accurate, the ionization potentials (obtained from the highest occupied orbital energies), excited states, and continuum states are not adequately described. For proper treatment of photoionization, MPI, and HHG processes, it is essential that both the ionization potentials and excited-state properties of atomic and molecular systems be described more accurately.

A promising procedure for removing the self-interaction energy in steady-state DFT treatments can be made based on the extension of the Krieger-Li-Iafrate (KLI) semianalytic treatment [8] of the optimized effective potential (OEP) formalism [9,10] along with the use of either the Hartree exchange [8,11] or an explicit self-interaction-correction (SIC) form [12,13]. As shown in recent works, the optimized effective potential so constructed has the proper long-range asymptotic $(-1/r)$ behavior and is capable of providing high accuracy for both excited and autoionizing resonance states [12,13]. Recently, the OEP/KLI-SIC formalism for the atomic and molecular systems has been extended to the time domain [2–4]. We note that a related time-dependent OEP/KLI formalism has been proposed [1] for the atomic systems in the exchange (x)- only limit. In the latter approach [1], the

Hartree-Fock (nonlocal) exchange functional form is used instead of the explicit SIC form [2–4] in the construction of the OEP. As shown in our recent works for atomic [2,3] and H_2 [4] systems, the use of explicit SIC form in the time-dependent OEP/KLI calculations involves only orbital-independent single-particle local potentials for each time step and is thus computationally efficient and yet maintains high accuracy.

An alternative and simpler approach to incorporate proper long-range potential in DFT calculations is suggested by van Leeuwen and Baerends (LB) [14]. They construct a model potential form (with Becke-like [15] *nonlocal* gradient correction to LSDA xc potential) that incorporates the general features of atomic-shell structure and asymptotic Coulomb behavior. The LB potential [14] and its modified version [17] has been used for a number of atomic and molecular electronic structure and weak-field photo-response calculations [16–18]. Comparing with the OEP/KLI- SIC method, the LB potential approach may not be as rigorous but it is simpler to use, particularly for the molecular systems, and it has demonstrated good accuracy. In this paper, we extend the modified LB model potential [17] in our TDDFT treatment of the multiphoton processes of N_2 molecules in intense laser fields.

The organization of this paper is as follows. First, we briefly describe the TDDFT formalism for the general treatment of multiphoton dynamics of many-electron molecular systems in Sec. II. Second, we outline a generalized pseudospectral method in Sec. III for *nonuniform* spatial discretization and electronic structure calculation of the two-center N_2 Hamiltonian. Third, we outline in Sec. IV a *time-dependent generalized pseudospectral* method for efficient and accurate solution of TDDFT equations in space and time. The method is then applied to the study of multiphoton ionization of N_2 in Sec. V and high-order harmonic generation of N_2 in Sec. VI. Particular attention is paid to the study of the dynamical role and nonlinear response of the individual valence electron to the external laser fields. This is followed by a conclusion in Sec. VII.

II. TIME-DEPENDENT DENSITY-FUNCTIONAL THEORY FOR N_2

Time dependent density functional theory (TDDFT) is based on the existence of the one-to-one correspondence between the time-dependent electron density and time-dependent potential [19]. We consider a quantum action integral

$$A=\int_{t_0}^{t_1} dt \left\langle \Psi(t)\left| i\frac{\partial}{\partial t}-\hat{H}(t)\right|\Psi(t)\right\rangle, \tag{1}$$

where $\Psi(t)$ is the total N-electron wave function

$$\Psi(t)=\frac{1}{\sqrt{N!}}\det[\psi_1\psi_2\cdots\psi_N], \tag{2}$$

and the total electron density at time t is determined by the set of occupied single-electron orbital wave functions $\{\psi_{i\sigma}\}$ as

$$\rho(\mathbf{r},t)=\sum_{\sigma}\sum_{i=1}^{N_\sigma}\psi_{i\sigma}^{*}(\mathbf{r},t)\psi_{i\sigma}(\mathbf{r},t). \tag{3}$$

The quantum action $A[\rho]$ has a *stationary* point at the *exact* time-dependent density of the system. From the Euler equation

$$\frac{\delta A[\rho(\mathbf{r},t)]}{\delta\rho_\sigma(\mathbf{r},t)}=0, \tag{4}$$

we get

$$\begin{aligned} i\frac{\partial}{\partial t}\psi_{i\sigma}(\mathbf{r},t)&=\hat{H}(\mathbf{r},t)\psi_{i\sigma}(\mathbf{r},t)\\ &=\left[-\frac{1}{2}\nabla^2+V_{eff,\sigma}([\rho];\mathbf{r},t)\right]\psi_{i\sigma}(\mathbf{r},t),\\ &\qquad i=1,2,\ldots,N_\sigma. \end{aligned} \tag{5}$$

Here,

$$V_{eff,\sigma}([\rho];\mathbf{r},t)=v_{ext}(\mathbf{r},t)+\int\frac{\rho(\mathbf{r}',t)}{|\mathbf{r}-\mathbf{r}'|}d^3\mathbf{r}'+v_{xc,\sigma}(\mathbf{r},t), \tag{6}$$

and $v_{ext}(\mathbf{r},t)$ is the ''external'' potential due to the interaction of the electron with the external laser field and the nuclei. In the case of the N_2 molecule in a linearly polarized external laser field, we have

$$v_{ext}(\mathbf{r},t)=-\frac{Z}{|\mathbf{R}_1-\mathbf{r}|}-\frac{Z}{|\mathbf{R}_2-\mathbf{r}|}+\mathbf{E}(t)\cdot\mathbf{r}\sin\omega t. \tag{7}$$

$\mathbf{r}$ is the electronic coordinate, E(t) the electric field amplitude, $\mathbf{R}_1=(0,0,a)$ and $\mathbf{R}_2=(0,0,-a)$ are the coordinates of the two nuclei in Cartesian coordinates, and Z is the nuclear charge. The internuclear separation R is equal to $2a$. $v_{xc\sigma}(\mathbf{r},t)$ is the time-dependent exchange-correlation (xc) potential. Since the exact form of $v_{xc\sigma}(\mathbf{r},t)$ is unknown, the *adiabatic* approximation is often used [1–6]

$$v_{xc\sigma}(\mathbf{r},t)=v_{xc\sigma}[\rho_\sigma]|_{\rho_\sigma=\rho_\sigma(\mathbf{r},t)}. \tag{8}$$

Note that if explicit xc energy functional forms from LSDA or GGA are used, the corresponding xc potential $v_{xc\sigma}(\mathbf{r},t)$ will not possess the correct long-range asymptotic $(-1/r)$ behavior. Here, we adopt the recently improved LB potential [17], $v_{xc\sigma}^{LB\alpha}$, which contains two empirical parameters α and β and that has the following form, in the adiabatic approximation,

$$v_{xc\sigma}^{LB\alpha}(\mathbf{r},t)=\alpha v_{x\sigma}^{LSDA}(\mathbf{r},t)+v_{c\sigma}^{LSDA}(\mathbf{r},t) - \frac{\beta x_\sigma^2(\mathbf{r},t)\rho_\sigma^{1/3}(\mathbf{r},t)}{1+3\beta x_\sigma(\mathbf{r},t)\ln\{x_\sigma(\mathbf{r},t)+[x_\sigma^2(\mathbf{r},t)+1]^{1/2}\}}. \quad (9)$$

Here, ρ_σ is the electron density with spin σ, and $\alpha=1.19$ and $\beta=0.01$. The first two terms in Eq. (9), $v_{x\sigma}^{LSDA}$ and $v_{c\sigma}^{LSDA}$ are the LSDA exchange and correlation potentials that do *not* have the correct asymptotic behavior. The last term in Eq. (9) is the nonlocal gradient correction with $x_\sigma(\mathbf{r})=|\nabla\rho_\sigma(\mathbf{r})|/\rho_\sigma(\mathbf{r})^{4/3}$, which ensures the proper long-range asymptotic $v_{xc\sigma}^{LB\alpha}\to -1/r$ as $r\to\infty$. For the time-independent case, this exchange-correlation LBα potential has been found to be reliable for the electronic structure and frequency-dependent (hyper) polarizability calculations of a number of atomic and molecular systems [16,17].

III. ELECTRONIC STRUCTURE CALCULATION OF N_2: GENERALIZED PSEUDOSPECTRAL DISCRETIZATION OF TWO-CENTER SYSTEMS

In this section, we first consider the solution of the field-free electronic structure calculations of N_2 using the generalized pseudospectral (GPS) method recently developed for the two-center systems [4]. We shall use the prolate spheroidal coordinates (μ,ν,ϕ), $0<\mu<\infty$, $0<\nu<\pi$, $0<\phi<2\pi$, for the description of the system

$$x=a\sinh\mu\sin\nu\cos\phi, \quad (10)$$

$$y=a\sinh\mu\sin\nu\sin\phi, \quad (11)$$

$$z=a\cosh\mu\cos\nu. \quad (12)$$

Due to the axial symmetry of the diatomic systems, the field-free solution takes the form

$$\Psi_m(\mathbf{r})=e^{im\varphi}\Phi(\mu,\nu), \quad (m=0,\pm1,\pm2,\ldots). \quad (13)$$

We first consider *nonuniform* optimal discretization of the spatial coordinates by means of the *generalized pseudospectral* (GPS) technique [21,22]. In the GPS method, we expand any spatial wave function $\Phi(\mu,\nu)$ by $\Phi_{N_\mu,N_\nu}(\mu,\nu)$, the polynomials of order N_μ and N_ν in μ and ν, respectively,

$$\Phi(\mu,\nu)\simeq\Phi_{N_\mu,N_\nu}(\mu,\nu) = \sum_{i=0,\,j=0}^{N_\mu,N_\nu}\phi(\mu_i,\nu_j)g_i(x(\mu))g_j(y(\nu)), \quad (14)$$

and further require the approximation to be exact at the collocation points, i.e., $\Phi_{N_\mu,N_\nu}(\mu_i,\nu_j)=\phi(\mu_i,\nu_j)\equiv\phi_{ij}$, where $\{x(\mu_i)\}$ and $\{y(\nu_j)\}$ are the two sets of collocation points to be described below. In Eq. (14), $g_i(x)$ and $g_j(y)$ are the cardinal functions [21–23] defined as

$$g_i(x)=-\frac{1}{N_\mu(N_\mu+1)P_{N_\mu}(x_i)}\frac{(1-x^2)P'_{N_\mu}(x)}{x-x_i}, \quad (15)$$

$$g_j(y)=-\frac{1}{N_\nu(N_\nu+1)P_{N_\nu}(y_j)}\frac{(1-y^2)P'_{N_\nu}(y)}{y-y_j}. \quad (16)$$

In the case of the Legendre pseudospectral method [4,21–23], which we adopt in this paper, the boundary points are $x_0=y_0=-1$ and $x_{N_\mu}=y_{N_\nu}=1$. x_i $(i=1,\ldots,N_\mu-1)$ and y_j $(j=1,\ldots,N_\nu-1)$ are the collocation points determined, respectively, by the roots of the first derivative of the Legendre polynomial P_{N_μ} with respect to x and the first derivative of P_{N_ν} with respect to y, namely,

$$P'_{N_\mu}(x_i)=0, \quad (17)$$

$$P'_{N_\nu}(y_j)=0. \quad (18)$$

It follows that the cardinal functions possess the following unique properties:

$$g_i(x_{i'})=\delta_{i,i'}, \quad (19)$$

$$g_j(y_{j'})=\delta_{j,j'}. \quad (20)$$

We shall use the following mapping relationships between μ and x and between ν and y [4]:

$$\mu=L\frac{1+x}{1-x}, \quad (21)$$

$$\nu=\frac{\pi}{2}(1+y), \quad (22)$$

where $x\in[-1,1]$, $y\in[-1,1]$, $\mu\in[0,\infty]$, $\nu\in[0,\pi]$, and L is a mapping parameter. The collocation points of $x(\mu)$ and $y(\nu)$ are determined by Eqs. (17) and (18).

A detailed discussion of the construction of the differentiation matrix and the symmetrization of the Hamiltonian matrix for two-center systems is given elsewhere [24]. A major advantage of the outlined generalized pseudospectral method is that it allows for *nonuniform* optimal spatial grid discretization: denser mesh near the nuclei and sparser mesh for the longer-range part of the Coulombic potential. With the use of only a modest number of grid points, high-precision eigenvalues and eigenfunctions may be obtained since the physically most important short-range regime is accurately treated. For example, for the case of H_2^+, we obtain the ground-state electronic energy to be $-1.102\,634\,214\,494\,9$ a.u., using only 22 points in μ and 10 points in ν [24]. This is in complete agreement with the exact value of $-1.102\,634\,214\,494\,9$ a.u. [20]. Figure 1 shows a typical grid structure for two-center diatomic systems.

The ground-state electronic configuration of N_2 is

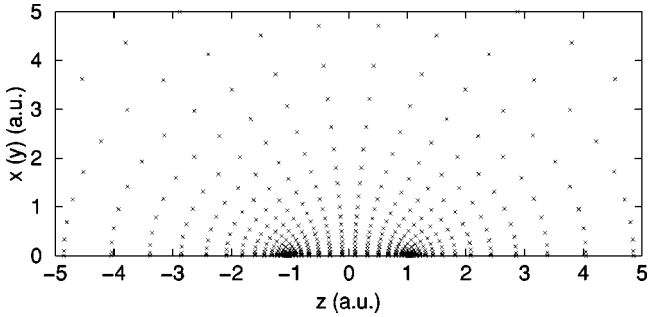

FIG. 1. A typical grid structure of the spatial coordinates of N_2 obtained by the generalized pseudospectral discretization technique.

$$1\sigma_g^2 1\sigma_u^2 2\sigma_g^2 2\sigma_u^2 1\pi_u^4 3\sigma_g^2.$$

According to the valence bond theory, this molecule has a triple bond formed with $3\sigma_g$ and $1\pi_u$ electrons. The $3\sigma_g$ orbital is parallel to the internuclear axis and the two degenerate $1\pi_u$ orbitals are perpendicular to it. Table I lists the orbital energies (ionization potentials) calculated with LBα potential [17] and LSDA and BLYP energy functionals, and the comparison of them with the experimental data. As shown, both the LSDA and BLYP orbital energies are too weakly bounded and considerably smaller than the experimental values. In contrast, the LBα orbital energies are considerably better since the LBα potential has the correct long-range $(-1/r)$ behavior.

IV. NUMERICAL SOLUTION OF THE TDDFT EQUATION: TIME-DEPENDENT GENERALIZED PSEUDOSPECTRAL METHOD

In this section, we outline the numerical procedure for the solution of the set of time-dependent equations Eq. (5) for N_2 molecule. The commonly used procedures for the time propagation of the Schrödinger or TDDFT equation employ *equal-spacing* spatial-grid discretization [1,25–27]. For processes such as high-harmonic generation (HHG) [2–4,28], accurate time-dependent wave functions are required to achieve convergence since the intensity of various harmonic peaks can span a range of many orders of magnitude. High-precision wave functions are generally more difficult to achieve by the equal-spacing spatial-grid-discretization time-dependent techniques, due to the Coulomb singularity at the origin and the long-range behavior of the Coulomb potential. To achieve precision time-dependent wave-function propagation, we have recently introduced a time-dependent generalized pseudospectral method for two-center systems [4], which consists of the following two basic elements: (i) A *generalized pseudospectral* (GPS) technique [21,22] is used for *nonuniform* optimal grid discretization of the radial coordinates: *denser* mesh near the nuclei and at short distances. The extension of the GPS method to the two-center systems has been described in the last section. (ii) A split-operator technique in the *energy* representation is introduced for efficient time propagation of the wave functions in two-center systems [4].

Consider now the solution of the time-dependent one-electron Kohn-Sham-like equation for N-electron systems in linearly polarized laser fields, Eq. (5),

$$i\frac{\partial}{\partial t}\psi_{i\sigma}(\mathbf{r},t)=\hat{H}\psi_{i\sigma}(\mathbf{r},t)=[\hat{H}_0(\mathbf{r})+\hat{V}(\mathbf{r},t)]\psi_{i\sigma}(\mathbf{r},t),$$

$$i=1,2,\ldots,N_\sigma. \quad (23)$$

Here, $\hat{H}_0$ is the time-independent Hamiltonian with $V_{eff,\sigma}$ set at $t=0$, and $\hat{V}$ includes the electron-laser field interaction and the residual time-dependent terms in $V_{eff,\sigma}([\rho];\mathbf{r},t)$

$$\hat{H}_0(\mathbf{r})=-\frac{1}{2a^2}\left\{\frac{1}{(\sinh^2\mu+\sin^2\nu)\sinh\mu}\frac{\partial}{\partial\mu}\left(\sinh\mu\frac{\partial}{\partial\mu}\right)+\frac{1}{(\sinh^2\mu+\sin^2\nu)\sin\nu}\frac{\partial}{\partial\nu}\left(\sin\nu\frac{\partial}{\partial\nu}\right)\right\}+V_{eff,\sigma}([\rho];\mathbf{r},0), \quad (24)$$

$$\hat{V}(\mathbf{r},t)=-\mathbf{E}(t)\cdot\mathbf{r}\sin\omega t+V_{eff,\sigma}([\rho];\mathbf{r},t)-V_{eff,\sigma}([\rho];\mathbf{r},0), \quad (25)$$

where $\mathbf{E}(t)$ is the electric field, assumed to be parallel to the internuclear $(\hat{\mathbf{z}})$ axis, and $E(t)=Ff(t)$, where $f(t)$ is the envelope function of the laser pulse. We shall extend the second-order split-operator technique in prolate spheroidal coordinates and in the *energy* representation [4,28] for the propagation of individual spin-orbital

$$\psi_{i\sigma}(\mathbf{r},t+\Delta t)\simeq e^{-i\hat{V}(\mathbf{r},t)\Delta t/2}e^{-i\hat{H}_0(\mathbf{r})\Delta t}e^{-i\hat{V}(\mathbf{r},t)\Delta t/2}\psi_{i\sigma}(\mathbf{r},t)+O(\Delta t^3). \quad (26)$$

Note that such an expression is different from the conventional split-operator techniques [25–27], where $\hat{H}_0$ is usually chosen to be the kinetic-energy operator and $\hat{V}$ the remaining Hamiltonian depending on the spatial coordinates only. The use of the *energy* representation in Eq. (26) allows the ex-

TABLE I. Comparison of the field-free energy levels of N_2 calculated with LBα, LSDA, and BLYP potentials and the experimental ionization potentials (in a.u.).

Orbital	$1\sigma_g$	$1\sigma_u$	$2\sigma_g$	$2\sigma_u$	$1\pi_u$	$3\sigma_g$
Experiments	15.0492 [31]	15.0492 [31]	1.3708 [32]	0.6883 [33]	0.6233 [33]	0.5726 [33]
LSDA	13.9655	13.9640	1.0395	0.4928	0.4379	0.3826
BLYP	14.1177	14.1166	1.0312	0.4936	0.4177	0.3751
LBα	14.7815	14.7804	1.2067	0.6679	0.6099	0.5571

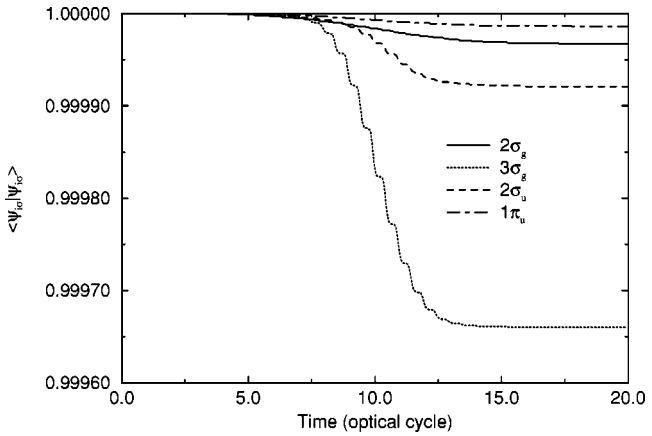

FIG. 2. The time-dependent population of electrons in different spin orbitals of N_2 in 10^{14} W/cm^2, 1064 nm, sin^2 pulse laser field with 20 optical cycles in pulse duration.

plicit *elimination* of the undesirable fast-oscillating *high-energy* components and speeds up considerably the time propagation [4,28]. In addition, the symmetry properties possessed by $\hat{H}_0$ can be used to simplify and facilitate the calculations. We refer to [4] for a more detailed discussion for the numerical procedure. After the time-dependent single-electron wave functions $\{\psi_{i\sigma}\}$ are obtained, the total electron density $\rho(t)$ may be determined.

V. MULTIPHOTON IONIZATION OF N_2 IN INTENSE LASER FIELDS

Once the time-dependent wave functions and the time-dependent electron density are obtained, we may calculate the time-dependent (multiphoton) ionization probability of the $i\sigma$th spin orbital according to

$$P_{i,\sigma}=1-N_{i,\sigma}(t), \tag{27}$$

where

$$N_{i\sigma}(t)=\langle\psi_{i,\sigma}(t)|\psi_{i,\sigma}(t)\rangle, \tag{28}$$

is the time-dependent population (survival probability) of the i,σth spin orbital.

Figures 2–4 present the time-dependent single-electron populations of different spin orbitals, as defined in Eq. (28). The slope of the decay of the electron population in time describes the ionization rate. The laser (electric) field is assumed to be parallel to the internuclear axis and the internuclear distance of N_2 is fixed at its equilibrium position, $R_e=2.072\,a_0$. Results for two laser intensities (10^{14} W/cm^2 and 3×10^{14} W/cm^2) and two wavelengths (1064 and 800 nm) are shown. For the case of 10^{14} W/cm^2, and for both wavelengths, the order of ionization probability is found to be

$$1\pi_u<2\sigma_g<2\sigma_u<3\sigma_g.$$

On the other hand, for the 3×10^{14} W/cm^2 and 1064 nm pulses, the order of ionization probability is

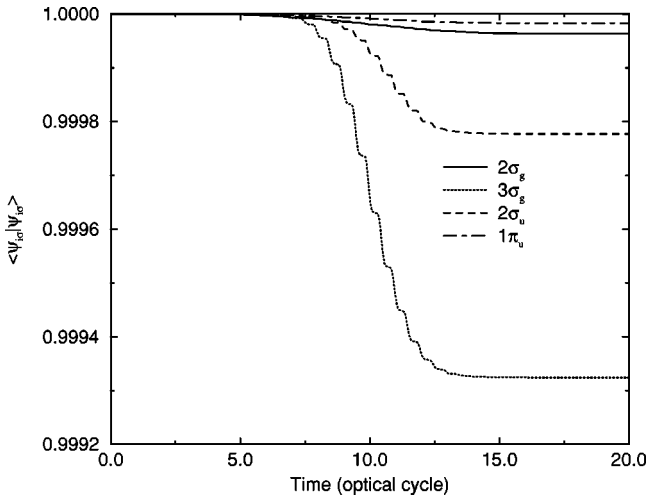

FIG. 3. The time-dependent population of electrons in different spin orbitals of N_2 in 10^{14} W/cm^2, 800 nm, sin^2 pulse laser field, with 20 optical cycles in pulse duration.

$$2\sigma_g<1\pi_u<2\sigma_u<3\sigma_g.$$

Thus, within the σ electrons, the lower the electron orbital binding energy (ionization potential) is, the more will be the electron ionization probability. However, although the ionization potential of the $1\pi_u$ electrons is lower than that of the $2\sigma_u$ electrons, the ionization probability of the $1\pi_u$ electrons turns out to be less than that of the $2\sigma_u$ electrons in all the cases. This may be attributed to the fact that the $2\sigma_u$ orbital is along the electric-field direction ($\hat{E}$), while that of $1\pi_u$ is perpendicular to $\hat{E}$. We thus observe two different effects that contribute to the ionization: the ionization potential (electron binding energy) effect and the orbital orientation effect. The ionization potential effect makes the electrons with lower-ionization potentials easier to ionize. The orientation effect makes the ionization easier for those electrons whose orbital orientations are parallel to the electric field. In

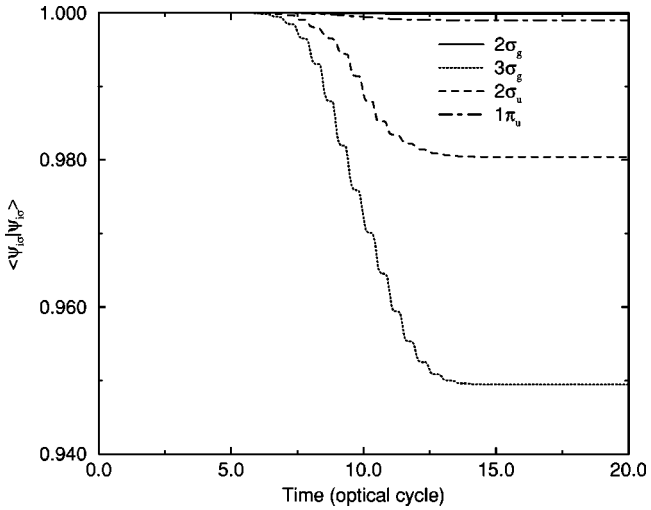

FIG. 4. The time-dependent population of electrons of N_2 molecule in different spin orbitals in 3×10^{14} W/cm^2, 1064 nm, sin^2 pulse laser field, with 20 optical cycles in pulse duration.

a related context, it has been found experimentally that linear molecules tend to align along the laser-field direction for dissociative ionization processes [29,30]. These two effects are clearly competing. For example, the ionization probability of the $1\pi_u$ electron is less than that of the $2\sigma_g$ electron in the 10^{14} W/cm^2 field, but the reverse is true in the 3×10^{14} W/cm^2 case, indicating that the increase of laser intensity tends to favor the ionization potential effect.

Finally we note that TDDFT studies of the nonlinear response of the individual spin orbital of complex rare-gas atoms (Ne,Ar) to intense laser fields have been recently reported [3]. Similar competing behavior of electron binding energy and orbital orientation effects on MPI and HHG was observed [3].

VI. HIGH-HARMONIC GENERATION OF N_2 IN INTENSE LASER FIELDS

The total induced dipole moment and dipole acceleration of N-electron systems may be expressed in terms of electron density ρ as follows:

$$d(t)=\int \rho(\mathbf{r},t)z\,d^3\mathbf{r}=\sum_{i\sigma}\langle\psi_{i\sigma}(\mathbf{r},t)|z|\psi_{i\sigma}(\mathbf{r},t)\rangle, \quad (29)$$

and

$$d_A(t)=\int \rho(\mathbf{r},t)\frac{d^2z}{dt^2}d^3\mathbf{r}$$
$$=\sum_{i\sigma}\left\langle\psi_{i\sigma}(\mathbf{r},t)\right|-\frac{\partial V_{eff,\sigma}([\rho];\mathbf{r},t)}{\partial z}$$
$$+\frac{\mathbf{E}(t)\cdot\mathbf{r}\sin(\omega t)}{z}\left|\psi_{i\sigma}(\mathbf{r},t)\right\rangle. \quad (30)$$

The corresponding HHG power spectrum may now be obtained by the Fourier transformation of the respective time-dependent dipole moment or dipole acceleration

$$P(\omega)=\left|\frac{1}{t_f-t_i}\int_{t_i}^{t_f}d(t)e^{-i\omega t}\right|^2\equiv|d(\omega)|^2, \quad (31)$$

and

$$P_A(\omega)=\left|\frac{1}{t_f-t_i}\frac{1}{\omega^2}\int_{t_i}^{t_f}d_A(t)e^{-i\omega t}\right|^2\equiv|d_A(\omega)|^2. \quad (32)$$

The total induced dipole moment may be rewritten as

$$d(t)=\sum_{i,\sigma}d_{i,\sigma}, \quad (33)$$

where

$$d_{i,\sigma}=n_{i,\sigma}\langle\psi_{i,\sigma}(t)|z|\psi_{i,\sigma}(t)\rangle, \quad (34)$$

is the induced dipole moment of the i,σth electron spin orbital, and $n_{i,\sigma}$ is its electron occupation number.

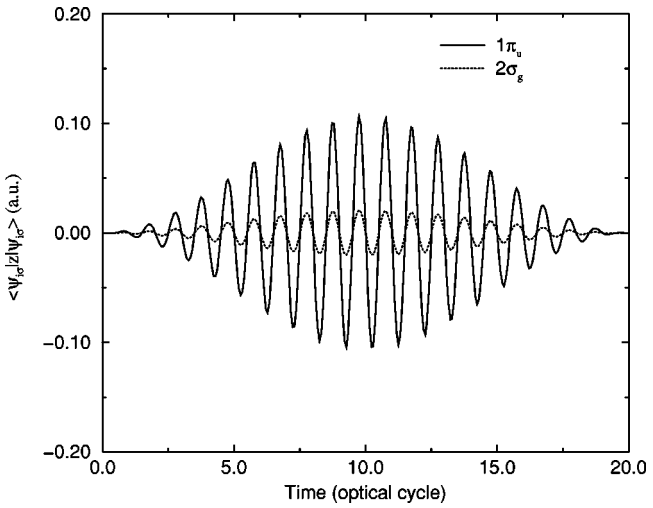

FIG. 5. The induced electronic dipole moment of N_2 calculated from $2\sigma_g$ and $1\pi_u$ electron, respectively, in 10^{14} W/cm^2, 1064 nm, sin^2 pulse laser field.

From Figs. 5–10, we present a series of $d_{i,\sigma}(t)$'s and $d(t)$'s as functions of time for the nonlinear response of the individual spin orbital of N_2 in 10^{14} W/cm^2 (1064 or 800 nm), sin^2 laser pulse, with 20 optical cycles in pulse length. The internuclear distance of N_2 is fixed at $R_e=2.072\,a_0$, and LBα model potential is used. For both 1064 and 800 nm cases, we found the amplitude of the induced dipole moment of individual spin orbital follows the following trend:

$$d_{2\sigma_g}<d_{1\pi_u}<d<d_{3\sigma_g}<d_{2\sigma_u}. \quad (35)$$

First, we note that electrons with smaller binding energies tend to have larger induced dipole moments. This is the case here for the bonding orbitals: $d_{2\sigma_g}<d_{1\pi_u}<d_{3\sigma_g}$. Second, the highest-occupied bonding ($3\sigma_g$) and antibonding ($2\sigma_u$) orbitals have comparable and largest induced dipole moments, with $d_{2\sigma_u}$ slightly higher in amplitude. Therefore, the in-

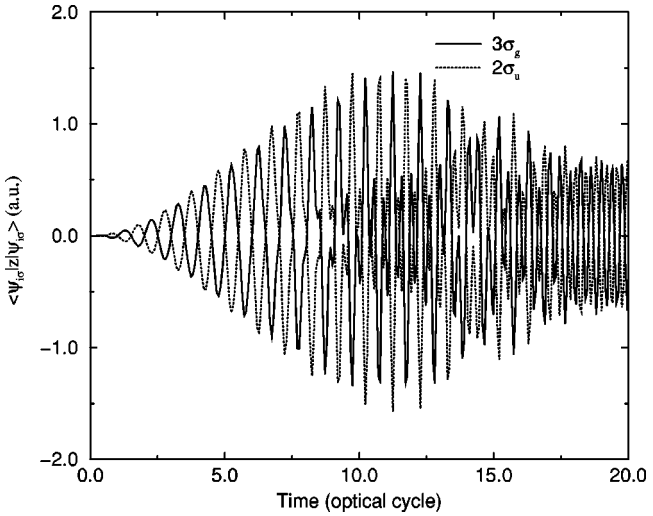

FIG. 6. The induced dipole moment of N_2 calculated from $3\sigma_g$ and $2\sigma_u$ electron, respectively, in 10^{14} W/cm^2, 1064 nm, sin^2 pulse laser field.

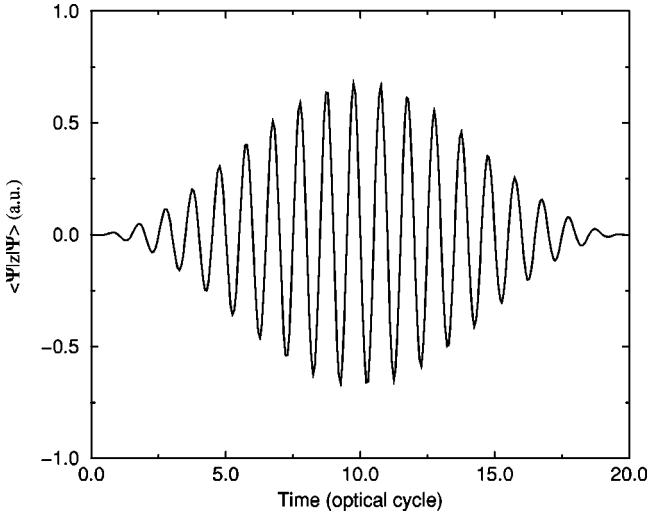

FIG. 7. The total induced dipole moment of N_2 in 10^{14} W/cm^2, 1064 nm, sin^2 pulse laser field.

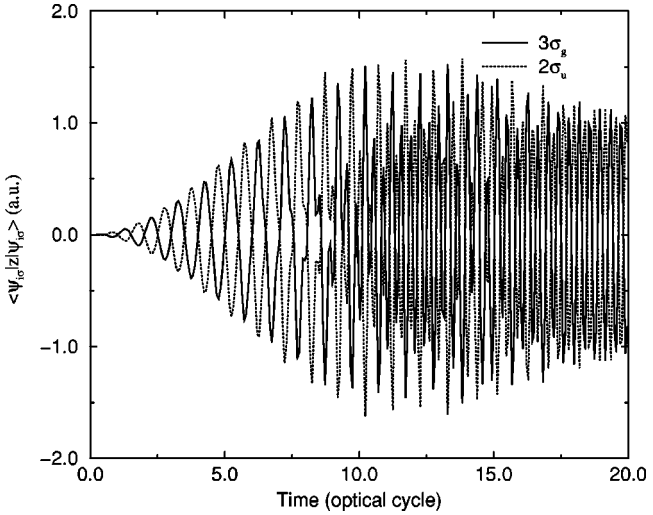

FIG. 9. The induced dipole moment of the $3\sigma_g$ and $2\sigma_u$ electrons of N_2 in 10^{14} W/cm^2, 800 nm, sin^2 pulse laser field.

duced dipole, similar to the ionization rate, also depends on the detailed electron density distribution of the spin orbitals. Third, there are two different oscillating ($+\hat{z}$ and $-\hat{z}$) directions of the electronic-induced dipoles. We found that $d_{2\sigma_g}$, $d_{1\pi_u}$, and $d_{2\sigma_u}$ are always oscillating in the same direction as that of the total induced dipole, while $d_{3\sigma_g}$ is always oscillating in the opposite direction (out of phase). Finally we notice that while $d_{3\sigma_g}$ and $d_{2\sigma_u}$ have similar amplitudes, they oscillate in time with opposite signs (Figs. 6 and 9). The near cancellation of these two largest induced dipole moments from $3\sigma_g$ and $2\sigma_u$ electrons results in a smaller total electronic induced dipole moment of the whole N_2 molecule shown in Figs. 7 and 10 for the case of 1064 and 800 nm, respectively.

Figure 11 shows the comparison of the HHG power spectra of N_2 in the 10^{14} W/cm^2, 1064 nm, sin^2 pulsed laser field, using two different xc potentials. The HHG spectra calculated with the LSDA and LBα potentials have considerable difference in amplitude due to their significant difference in the orbital binding energies (See Table I). This indicates the importance of incorporating the correct asymptotic long-range potential in the TDDFT treatment of strong field processes.

In order to study the relative contribution of the individual spin orbital to the overall harmonic generation, we substitute Eq. (33) into Eq. (31) to obtain

$$P(\omega)=\left|\sum_{i,\sigma}\frac{1}{t_f-t_i}\int_{t_i}^{t_f}d_{i,\sigma}e^{-i\omega t}dt\right|^2$$

$$=\sum_{i,\sigma}d_{i\sigma}(\omega)+\sum_{ij\alpha\beta}P_{ij,\alpha\beta}(\omega). \qquad (36)$$

Here,

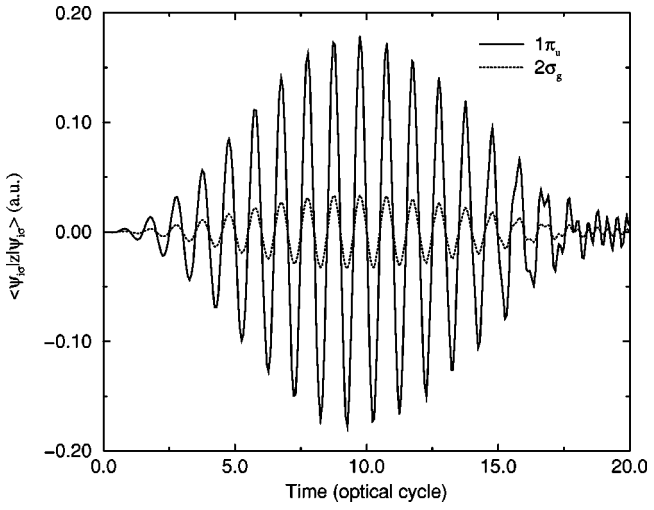

FIG. 8. The induced dipole moment of N_2 calculated from $2\sigma_g$ and $1\pi_u$ electron, respectively, in 10^{14} W/cm^2, 800 nm, sin^2 pulse laser field.

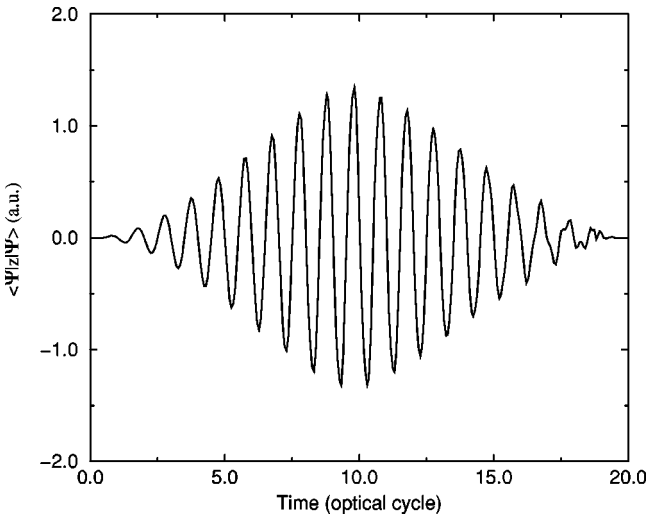

FIG. 10. The total induced dipole moment of N_2 in 10^{14} W/cm^2, 800 nm, sin^2 pulse laser field.

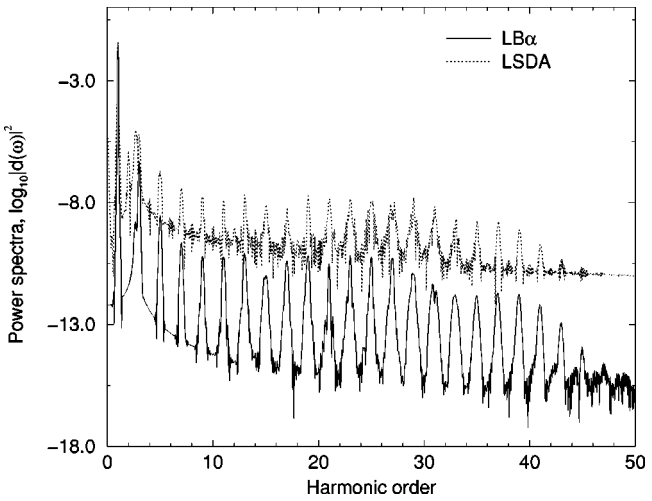

FIG. 11. Comparison of the calculated high-harmonic generation power spectra of N_2 in 10^{14} W/cm^2, 1064 nm, sin^2 pulse laser field, using LBα and LSDA potentials.

$$d_{i\sigma}(\omega)=\left|\frac{1}{t_f-t_i}\int_{t_i}^{t_f}d_{i,\sigma}e^{-i\omega t}dt\right|^2, \tag{37}$$

and

$$P_{ij,\alpha\beta}(\omega)=\left(\frac{1}{t_f-t_i}\int_{t_i}^{t_f}d_{i,\alpha}e^{-i\omega t}dt\right)^* \times\left(\frac{1}{t_f-t_i}\int_{t_i}^{t_f}d_{j,\beta}e^{-i\omega t}dt\right), \tag{38}$$

where i and j denote the orbital indices and α and β are the spin indices.

We now discuss the results of our *all-electron* HHG calculations of N_2. Again, the internuclear distance is fixed at $R_e=2.072\,a_0$ and the LBα potential is incorporated in the TDDFT calculations. The relative contribution of the individual spin orbital to HHG, $d_{i\sigma}(\omega)$, depends on the harmonic frequency range but in general, it follows roughly the same trend as the order of the time-dependent induced dipole shown in Eq. (35). Thus, the two dominant contributions to the total HHG arises from the $3\sigma_g$ and $2\sigma_u$ orbitals and in fact we found that the magnitude of their individual power spectrum is considerably larger than that of the total HHG itself. Equation (36) shows that the total HHG power spectrum is obtained by the sum of the individual spin-orbital HHG power spectrum $d_{i\sigma}(\omega)$ plus the interference terms. Thus, for the case of N_2, we observe very interesting constructive and destructive interferences between the two highest-occupied bond and antibonding orbitals: *It is the interference between these two largest induced dipoles* ($d_{3\sigma_g}$ *and* $d_{2\sigma_u}$) *that contributes dominantly to the overall* HHG *power spectrum of* N_2. This is illustrated in Figs 12 and 13 for the case of 1064 and 800 nm, respectively. Here, we compare the total HHG power spectra with those from the combined contributions from $3\sigma_g$ and $2\sigma_u$ orbitals alone. As seen, the total and $3\sigma_g+2\sigma_u$ HHG curves agree with each other fairly well for both laser frequencies. Thus, for many-electron molecular systems such as N_2, the conventional *single-active-electron* model for atoms is not valid, since there is no single electron molecular orbital dominates the total HHG process. In fact, our study shows that the total N_2 power spectrum is due to the interference contributions from the two highest-bonding and antibonding molecular orbitals.

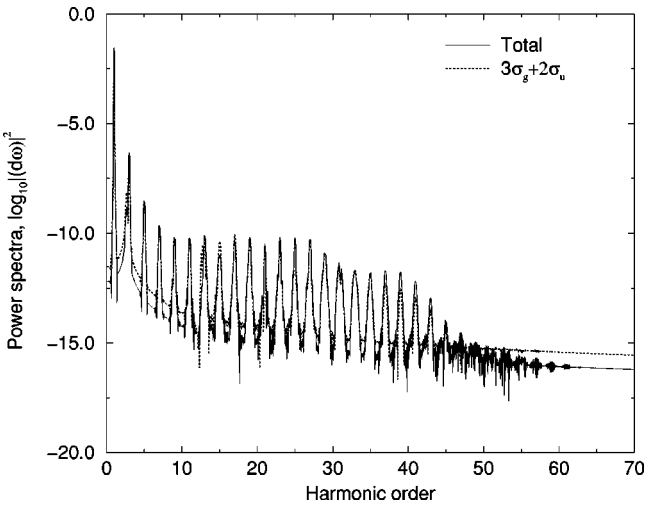

FIG. 12. Comparison of the total HHG power spectra and the partial contributions from the $3\sigma_g$ and $2\sigma_u$ orbitals of N_2, in 10^{14} W/cm^2, 1064 nm, sin^2 pulse laser field.

VII. CONCLUSIONS

The following conclusions can be drawn from the present TDDFT study of the multiphoton dynamics of N_2. First, correct long-range behavior of the time-dependent exchange and correlation potential is essential. Second, there coexists ionization potential and orbital orientation effects in the multiphoton ionization of multielectron systems. As the laser intensity increases, the ionization potential effect becomes dominant. Finally, the HHG of the N_2 molecule, especially

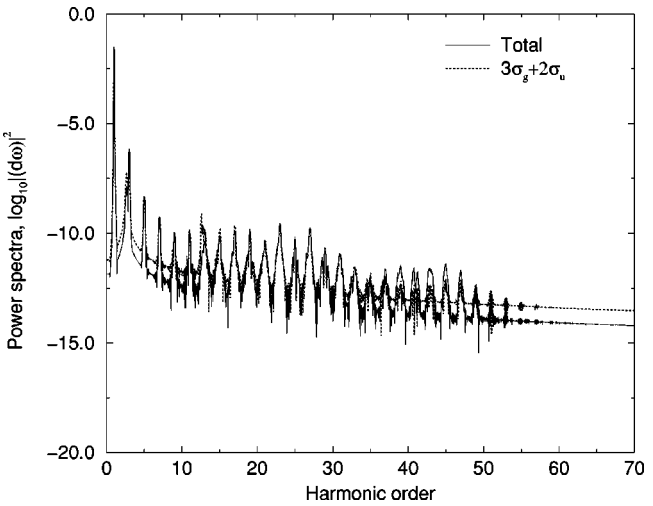

FIG. 13. Comparison of the total HHG power spectra and the partial contributions from $3\sigma_g$ and $2\sigma_u$ orbitals of N_2 in 10^{14} W/cm^2, 800 nm, sin^2 laser pulse.

below the cutoff regime, is primarily due to the combined interference dynamics of the highest-binding ($3\sigma_g$) and antibonding ($2\sigma_u$) electrons together. To our knowledge, this is the first *ab initio all-electron* quantum study of multielectron molecules in strong fields. Much more remains to be explored in this fascinating and largely unexplored area of strong-field molecular physics. Finally, the nuclear degree of freedom has not been taken into account so far. Research in these directions will be pursued in the future.

ACKNOWLEDGMENTS

This work was partially supported by the U.S. Department of Energy, Office of Science, Office of Basic Energy Sciences, Division of Chemical Sciences. We acknowledge the support of the Origin 2400 supercomputer time by the Kansas Center for Advanced Scientific Computing.

[1] C.A. Ullrich, U.J. Gossmann, and E.K.U. Gross, Phys. Rev. Lett. **74**, 872 (1995).
[2] X.M. Tong and S.I. Chu, Phys. Rev. A **57**, 452 (1998).
[3] X.M. Tong and S.I. Chu, Phys. Rev. A **64**, 013417 (2001).
[4] X. Chu and S.I. Chu, Phys. Rev. A **63**, 023411 (2001).
[5] E.K.U. Gross and W. Kohn, Adv. Quantum Chem. **21**, 255 (1990).
[6] G. Vignale and M. Rasolt, Phys. Rev. Lett. **59**, 2360 (1987).
[7] See, for example, R. Parr and W. Yang, *Density-Functional Theory of Atoms and Molecules* (Oxford University Press, New York, 1989).
[8] J.B. Krieger, Y. Li, and G.J. Iafrate, Phys. Lett. A **146**, 256 (1990).
[9] R.T. Sharp and G.K. Horton, Phys. Rev. **90**, 317 (1953).
[10] J.D. Talman and W.F. Shadwick, Phys. Rev. A **14**, 36 (1976).
[11] T. Grabo and E.K.U. Gross, Chem. Phys. Lett. **240**, 141 (1995).
[12] X.M. Tong and S.I. Chu, Phys. Rev. A **55**, 3406 (1997).
[13] X.M. Tong and S.I. Chu, Phys. Rev. A **57**, 855 (1998).
[14] R. van Leeuwen and E.J. Baerends, Phys. Rev. A **49**, 2421 (1994).
[15] A.D. Becke, Phys. Rev. A **38**, 3098 (1988).
[16] S.J.A. van Gisbergen *et al.*, Phys. Rev. A **57**, 2556 (1998).
[17] P.R.T. Schipper *et al.*, J. Chem. Phys. **112**, 1344 (2000).
[18] A. Banerjee and M.K. Harbola, Phys. Rev. A **60**, 3599 (1999).
[19] M.M. Madsen and J.M. Peek, At. Data **2**, 176 (1971).
[20] E. Runge and E.K.U. Gross, Phys. Rev. Lett. **52**, 997 (1984).
[21] G. Yao and S.I. Chu, Chem. Phys. Lett. **204**, 381 (1993).
[22] J. Wang, S.I. Chu, and C. Laughlin, Phys. Rev. A **50**, 3208 (1994).
[23] C. Canuto, M. Y. Hussaini, A. Quarteroni, and T. A. Zang, *Spectral Methods in Fluid Dynamics* (Springer, Berlin, 1988).
[24] X. Chu and S.I. Chu, Phys. Rev. A **63**, 013414 (2001).
[25] M.R. Hermann and J.A. Fleck, Jr., Phys. Rev. A **38**, 6000 (1988).
[26] T.F. Jiang and S.I. Chu, Phys. Rev. A **46**, 7322 (1992).
[27] K.C. Kulander, Phys. Rev. A **36**, 2726 (1987).
[28] X.M. Tong and S.I. Chu, Chem. Phys. **217**, 119 (1997).
[29] K. Codling and L.J. Frasinski, J. Phys. B **26**, 783 (1993).
[30] J.H. Posthumus *et al.*, J. Phys. B **29**, L525 (1996).
[31] G. Johansson, J. Hedman, A. Berndtsson, M. Klasson, and R. Nilsson, J. Electron Spectrosc. Relat. Phenom. **2**, 295 (1973).
[32] H. Hamnett, W. Stoll, and C.E. Brion, J. Electron Spectrosc. Relat. Phenom. **8**, 367 (1976).
[33] D.W. Turner, C. Baker, A.D. Baker, and C.R. Brundle, *Molecular Photoelectron Spectroscopy* (Wiley-Interscience, London, 1970).